



# One-step non-hydrolytic sol–gel preparation of efficient V<sub>2</sub>O<sub>5</sub>–TiO<sub>2</sub> catalysts for VOC total oxidation

Damien P. Debecker<sup>a</sup>, Karim Bouchmella<sup>b</sup>, Romain Delaigle<sup>a</sup>, Pierre Eloy<sup>a</sup>, Claude Poleunis<sup>c</sup>, Patrick Bertrand<sup>c</sup>, Eric M. Gaigneaux<sup>a</sup>, P. Hubert Mutin<sup>b,\*</sup>

<sup>a</sup> Université catholique de Louvain, Unité de catalyse et chimie des matériaux divisés, Croix du Sud 2/17, B-1348 Louvain-la-Neuve, Belgium

<sup>b</sup> Institut Charles Gerhardt, UMR 5253, CNRS-UM2-ENSCM-UM1, Université de Montpellier 2, cc 1701, Montpellier 34095, France

<sup>c</sup> Unité de physico-chimie et de physique des matériaux, Université catholique de Louvain, Croix du Sud 1, B-1348 Louvain-la-Neuve, Belgium

## ARTICLE INFO

### Article history:

Received 8 September 2009

Received in revised form 12 October 2009

Accepted 17 October 2009

Available online 29 October 2009

### Keywords:

Alkoxide

PCDD

PCDF

Air pollution

SCR

Nonhydrolytic

## ABSTRACT

Vanadia-titania catalysts are highly regarded for the control of industrial and domestic gas effluents. They are particularly used for the abatement of volatile organic compounds and for the removal of aromatic, polyaromatic and polychlorinated air pollutants like furans and dioxins. Here, mixed oxide catalysts are formed by non-hydrolytic condensation of chloride precursors with diisopropyl ether in non-aqueous medium. Calcination was applied to provoke the migration of the vanadium oxide toward the surface of the anatase particles, leading to well-spread vanadia species. The materials are made of mesoporous spherical particles of a few microns, themselves constituted by the aggregation of 10–25 nm sized particles. Their chemical composition is precisely controlled. The samples are characterized by ICP-AES, N<sub>2</sub>-physisorption, XRD, XPS, SEM and TOF-SIMS. Their performances as total oxidation catalyst are evaluated in the deep oxidation of benzene, chosen as a model atmospheric pollutant. The activity of the materials compares well with that of catalysts prepared by classical wet impregnation. Along with the V surface concentration, the environment in which V surface species are located is identified as a key parameter. The superior activity of polymeric species as compared to isolated ones is shown.

© 2009 Elsevier B.V. All rights reserved.

## 1. Introduction

V<sub>2</sub>O<sub>5</sub>-based catalysts are well-known total oxidation catalysts and they are widely used for the abatement of various air pollutants including aromatics, chlorinated aromatics, furans and dioxins [1]. Growing environmental concerns about atmospheric air pollution have spawned numerous fundamental and applied studies on these systems [2–12]. Gas effluents of incinerator or cogeneration plants must comply with stringent limitations on various types of harmful pollutants, including volatile organic compounds [13]. Supported vanadium oxide is reported as a very active catalyst, resistant against chlorine poisoning [14], which makes it also suitable for the abatement of chloro-aromatics including dioxins [15].

Supported V<sub>2</sub>O<sub>5</sub> catalysts are usually prepared by one-step or multi-step wet impregnation on titania supports. Increased performances can be obtained by co-impregnation of promoting oxides (Mo, W) [16–18], by changing the properties of the support [19] or by doping the V<sub>2</sub>O<sub>5</sub> active phase with metal nanoparticles [20]. However, classical preparation methods suffer from several

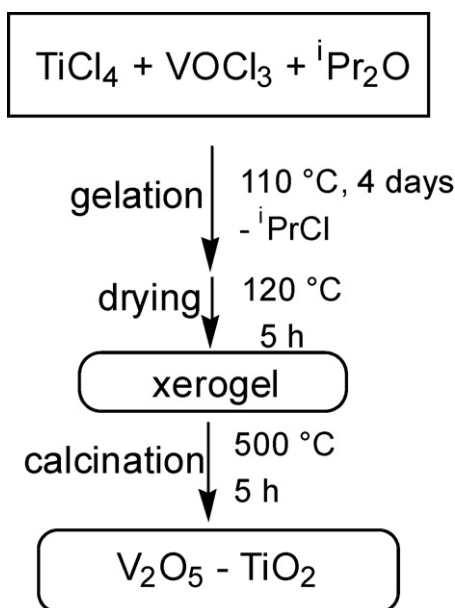
limitations. They involve at least two separate steps: the preparation of the support and the deposition of the active phase. The support may of course be purchased but the limited choice of commercial titania supports offers few possibilities to chose the most appropriate textural and surface properties of the material, even though these may impact the performance of the catalyst. Furthermore, the wet impregnation technique produces large amount of waste water which is not in accordance with current environmental concerns. Finally, the deposition of the vanadium precursor on the TiO<sub>2</sub> support during the drying step does not occur homogeneously. Controlling precisely the nature of the surface vanadium species and obtaining high dispersion is thus delicate with impregnation methods [21]. Consequently, several alternative techniques have been explored for the production of TiO<sub>2</sub>-V<sub>2</sub>O<sub>5</sub> catalysts, including flame spray pyrolysis [22], flame aerosol synthesis [23] and hydrolytic sol–gel processing [24–28].

Elaborated procedures have been developed with the aim to increase the activity of Ti/V sol–gel catalysts, such as multi-step synthesis or chemical modification to improve the dispersion of V species, and supercritical drying to improve the texture of the catalysts [25,29–32]. Ternary oxide catalysts have also been investigated: V-Ti-Si [33], V-Ti-Nb [34], V-Ti-W [26], V-Mo-Ti [35].

Recently, TiO<sub>2</sub>-V<sub>2</sub>O<sub>5</sub> catalysts exhibiting outstanding performance in the selective catalytic reduction of NO by ammonia were

\* Corresponding author. Tel.: +33 4 6714 3970; fax: +33 4 6714 3852.

E-mail address: [hubert.mutin@univ-montp2.fr](mailto:hubert.mutin@univ-montp2.fr) (P.H. Mutin).



**Scheme 1.** Schematic representation of the non-hydrolytic sol-gel preparation method.

synthesized using non-hydrolytic sol-gel [36]. Few characterizations were however reported concerning these systems. Since then, non-hydrolytic sol-gel chemistry has proven successful for the preparation different kinds of mixed oxides with a good control on composition and texture [37]. Very recently, non-hydrolytic routes have been successfully applied to the preparation of  $\text{SiO}_2$ - $\text{TiO}_2$  oxidation catalysts [38,39] or  $\text{SiO}_2$ - $\text{Al}_2\text{O}_3$ - $\text{MoO}_3$  metathesis catalysts [40].

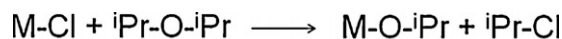
In this paper, the non-hydrolytic sol-gel route is exploited to prepare  $\text{V}_2\text{O}_5$ - $\text{TiO}_2$  catalysts dedicated to the total oxidation of volatile organic compounds (VOC) and the nature of the surface species produced by this non-conventional route is described in detail.

In order to maximize the activity of the catalysts, we used the following strategy: mesoporous xerogels were first prepared in a single step by reaction of the metal chlorides with diisopropyl ether, followed by vacuum drying. Then a controlled calcination step was applied in order to remove organic and chloride groups and to provoke the migration of V oxide species toward the catalyst surface (Scheme 1), taking advantage of the low Tammann temperature of vanadium oxide [25,40]. This strategy was monitored by XPS, TOF-SIMS and XRD. The performances were measured in the catalytic total oxidation of benzene to validate this innovative non-hydrolytic sol-gel route for the synthesis of tailored VOC abatement catalysts. Benzene has been chosen as a representative model for various air pollutants; it has also been widely used for modelling dioxins, even though in that case other compounds must also be used to complete the picture [41,42].

## 2. Experimental

### 2.1. Preparation of the catalysts

Manipulations were carried out under argon atmosphere in a glove box using glass tubes (80 ml). The xerogels were obtained by heating the reactants under autogenous pressure in a sealed tube (heavy-wall Pyrex tube). Diisopropyl ether ( $i\text{Pr}_2\text{O}$ , Acros Organics, 99%) was dried by distillation over sodium wire. Dichloromethane ( $\text{CH}_2\text{Cl}_2$ , VWR, 100%) was dried under pentaoxide diphosphorus ( $\text{P}_2\text{O}_5$ ). Vanadyl chloride ( $\text{VOCl}_3$ , Aldrich, 99%) and titanium chloride ( $\text{TiCl}_4$ , Acros Organics, 99.9%) were introduced first. The



**Scheme 2.** Reactions involved in the non-hydrolytic sol-gel route used. M can be Ti or V.

stoichiometric amount of  $i\text{Pr}_2\text{O}$  was added and finally 20 ml of  $\text{CH}_2\text{Cl}_2$ . The glass tube was frozen in liquid nitrogen and then sealed under vacuum. The sealed tube was heated at 110 °C in an oven for 4 days under autogenous pressure, leading to dark brown gels. The gelation involves the intermediate formation of isopropoxide groups that further condense with the remaining chloride groups with production of isopropyl chloride (Scheme 2). The resulting gel was dried under vacuum at 120 °C for 5 h (in order to eliminate  $i\text{PrCl}$ ). The obtained xerogels are then calcined under air at 500 °C for 5 h (heating rate 1 °C  $\text{min}^{-1}$ ). Catalysts are denoted SG- $\text{TiV}_x$ , where x represent the nominal weight loading of  $\text{V}_2\text{O}_5$ , in %.  $\text{V}_2\text{O}_5$  nominal loadings of 3, 5 and 10 wt% were explored.

The reference catalyst has been prepared by a classical wet impregnation method (WI) and is hereafter denoted WI- $\text{TiV}_5$ . The support is a 70% anatase-30% rutile  $\text{TiO}_2$  (Degussa P25; 49  $\text{m}^2/\text{g}$ ).  $\text{NH}_4\text{VO}_3$  (Vel; 99.9%) was used as V precursors. The precursor was dissolved in distilled water and complexed with 2 mol of oxalic acid (Aldrich, 98%) for 1 mol of transition metal. The obtained solid was dried overnight in an oven at 110 °C and then calcined at 400 °C at atmospheric pressure in air for 20 h in a muffle furnace. Details about the impregnation method can be found ref. [19].

### 2.2. Catalytic tests

Catalytic tests were performed in an inconel fixed-bed micro-reactor of 1 cm internal diameter (PID ENG&Tech, Spain, Madrid) operating at atmospheric pressure. The catalytic bed was composed of 200 mg of catalyst powder selected within the 200–315  $\mu\text{m}$  granulometric fraction and diluted in 800 mg of inactive glass spheres with diameters in the range 315–500  $\mu\text{m}$ . The gas stream contained 100 ppm of benzene in He (Praxair), 20% of  $\text{O}_2$  (Praxair; 99.995%) and He (Praxair; 99.996%) as diluting gas to obtain 200 ml/min (space velocity (VVH) = 37000  $\text{h}^{-1}$ ). The reaction was run from 100 to 400 °C in a step mode with a 150 min plateau at each temperature investigated. Analysis of reactants and products was continuously performed by on-line gas chromatography (GC). A CP-3800 gas chromatography apparatus from Varian equipped with four columns (one Haysep G, one Haysep T, one Molsieve and one CP-Sil 8CB) and three detectors (one TCD and two FID) was used with He as carrier gas in order to quantify benzene,  $\text{O}_2$ , CO,  $\text{CO}_2$  and to verify that no other hydrocarbon was formed. The analysis parameters were set as to allow each analysis 15 min and to obtain measurements accurate within about 1% (relative) for the conversion of benzene. To calculate the conversion at a given temperature, only the concentrations of reactants measured and averaged over the period of time from 100 to 150 min of each temperature plateau were taken into account. The conversion is defined as the ratio reactant transformed/reactant in the inlet (in %).

### 2.3. Characterization

X-ray diffraction (XRD) measurements were performed on the catalysts with a Siemens D5000 diffractometer using the  $\text{K}\alpha$  radiation of Cu ( $\lambda = 1.5418 \text{ \AA}$ ). The Debye-Scherrer equation was used to estimate the size of the anatase domains from the width of the 25.3° anatase peak. The crystallites were considered to be spherical and the peak width for a reference quartz crystal was 0.1°.

The weight percentages of V and Ti were measured by inductively coupled plasma-atomic emission spectroscopy (ICP-AES) on an Iris Advantage apparatus from Jarrell Ash Corporation.

N<sub>2</sub>-physisorption experiments were performed at −196 °C on a Micromeritics Tristar. The samples were outgassed for 6 h at 200 °C under vacuum (2 Pa). The pore size distribution was derived from the desorption branch using the BJH method.

X-ray photoelectron spectroscopy (XPS) analyses were performed on a SSX 100/206 photoelectron spectrometer from Surface Science Instruments (USA) equipped with a monochromatised microfocus Al X-ray source (powered at 20 mA and 10 kV). The samples powders pressed in small stainless steel troughs of 4 mm diameter were placed on a ceramic carousel. The pressure in the analysis chamber was around 10<sup>−6</sup> Pa. The angle between the surface normal and the axis of the analyzer lens was 55°. The analysed area was approximately 1.4 mm<sup>2</sup> and the pass energy was set at 150 eV. In these conditions, the resolution determined by the full width at half maximum (FWHM) of the Au 4f<sub>7/2</sub> peak was around 1.6 eV. A flood gun set at 10 eV and a Ni grid placed 3 mm above the sample surface were used for charge stabilisation. Following sequence of spectra was recorded: survey spectrum, C 1s, O 1s together with V 2p, Ti 2p, Cl 2p and C 1s again to check the stability of charge compensation in function of time and the absence of degradation of the sample during the analyses. The binding energies were calculated with respect to the C–(C,H) component of the C 1s peak fixed at 284.8 eV. Data treatment was performed with the CasaXPS program (Casa Software Ltd, UK), some spectra were decomposed with the least squares fitting routine provided by the software with a Gaussian/Lorentzian (85/15) product function and after subtraction of a non-linear baseline. Molar fractions were calculated using peak areas normalized on the basis of acquisition parameters and sensitivity factors provided by the manufacturer.

Scanning electron micrographs were obtained with a HITACHI-S4800 electron microscope.

Static positive and negative TOF-SIMS measurements were performed with a TOF-SIMS spectrometer from Charles Evans and Associates [43]. The sample was bombarded with pulsed Ga<sup>+</sup> ions (15 keV). The secondary ions were accelerated to ±3 keV by applying a bias on the sample. The spreading of the initial energies of the secondary ions is compensated by deflection in three electrostatic analyzers. A post-acceleration of 7 keV was applied at the detector entry. The analyzed area used in this work was a square of 120 μm × 120 μm and the data acquisition time was 5 min. Charge effects were compensated by means of a pulsed electron flood gun (*E<sub>k</sub>* = 24 eV). With these experimental settings the total ion fluence is lower than 10<sup>12</sup> Ga<sup>+</sup>/cm<sup>2</sup>, which ensures static conditions [43]. The

**Table 1**

Textural properties of the samples.

Generic name	SSA (m <sup>2</sup> g <sup>−1</sup> ) <sup>a</sup>	Pore diameter (nm) <sup>b</sup>	Pore volume (cm <sup>3</sup> g <sup>−1</sup> ) <sup>b</sup>
SG-TiV3	88	10.9	0.32
SG-TiV5	64	10.7	0.18
SG-TiV10	71	11.5	0.22
TiO <sub>2</sub> (P25)	49 <sup>c</sup>	–	–
WI-TiV5	46 <sup>c</sup>	–	–

<sup>a</sup> Specific surface areas were calculated by the BET method.

<sup>b</sup> Pore diameters and pore volumes were calculated by the BJH method applied on the desorption isotherm.

<sup>c</sup> Data taken from ref [41].

powders were pressed on a double-face silver tape. A stainless steel grid (non-magnetic) was placed onto the sample surface in order to prevent variations of the surface potential.

### 3. Results

#### 3.1. Catalyst characterization

The reference WI catalyst had a specific surface area (SSA) of 46 m<sup>2</sup> g<sup>−1</sup>, which is slightly lower than the SSA of the bare support (49 m<sup>2</sup> g<sup>−1</sup>) [41]. SG catalysts all had a specific surface area (SSA) in the same order but typically higher, from 64 to 88 m<sup>2</sup> g<sup>−1</sup> (Table 1). N<sub>2</sub> adsorption–desorption isotherms were always of type IV, according to the BDDT classification, confirming that all SG samples were mesoporous. A representative example is given in Fig. 1; the pores had a mean diameter of about 10 nm with a quite narrow pore size distribution.

ICP-AES elementary analysis was used to verify the agreement between the final composition of the SG materials and the expected compositions (Table 2). The content in V is also given for the WI catalysts. The experimental weight percentages of Ti and V are in excellent agreement with the expected values calculated from the precise amount of reactant involved in each preparation.

Fig. 2 presents typical SEM micrographs obtained with non-hydrolytic sol–gel made samples. All SG catalysts may be described as aggregates of spherical particles of about 2–5 μm and sometimes partially fused together (Fig. 2a). The surface of these spheres appears to be very smooth in Fig. 2b. However, the size of these structures is not consistent with the specific surface area developed by the samples, meaning that each sphere is actually porous and constituted by an aggregation of smaller particles. At higher magnification indeed, it appears clearly that the big spherical particles are actually made of an agglomeration of

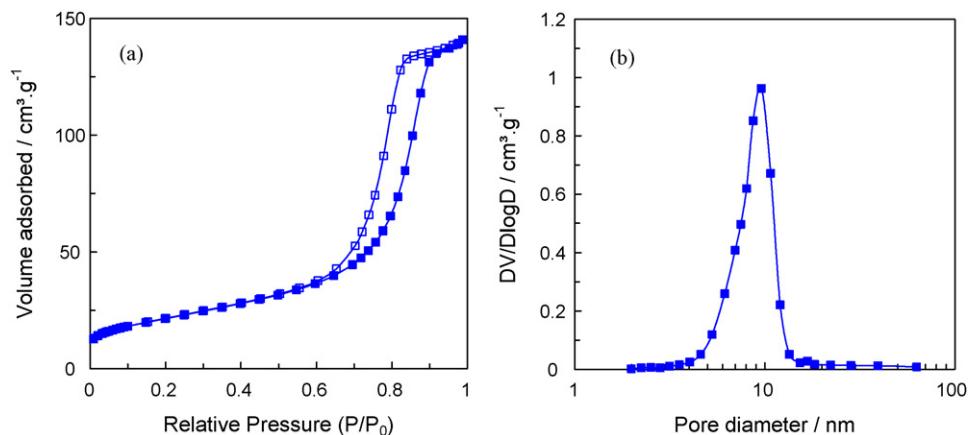


**Fig. 1.** N<sub>2</sub>-physisorption isotherms (a) and pore size distribution (b) obtained on TiV5. In the isotherms, filled and open symbols correspond to the adsorption and desorption branches, respectively.

**Table 2**

Experimental chemical composition (ICP-AES). The values given in brackets correspond to the expected wt% calculated from the amount of reactant involved in each SG preparation.

Generic name	Ti (wt%)	V (wt%)
SG-TiV3	58.4 (58.4)	1.5 (1.5)
SG-TiV5	57.2 (57.3)	2.6 (2.5)
SG-TiV10	53.6 (53.8)	5.9 (5.8)
WI-TiV5	56.7 <sup>a</sup>	2.6 <sup>a</sup>

<sup>a</sup> Data taken from ref [41].

smaller particles (Fig. 2c). The size of these small particles is always within the rough 10–25 nm range (Fig. 2d).

Fig. 3 shows that the SG samples only exhibited diffraction peaks related to the presence of the anatase phase (main peaks at  $2\theta = 25.3^\circ$ ,  $37.0^\circ$ ,  $37.8^\circ$ ,  $38.6^\circ$ ,  $48.1^\circ$ ,  $53.9^\circ$ ,  $55.1^\circ$ ,  $62.6^\circ$  following JCPDS 21-1272). No crystalline vanadium oxide is detected even for the maximum loading (10 wt%  $V_2O_5$ ). The diffractogram of the catalysts prepared by wet impregnation on the commercial support confirms the additional presence of rutile (main peaks at  $27.5^\circ$ ,  $36.2^\circ$ ,  $55.0^\circ$  following JCPDS 21-1276) in addition to anatase, as announced by the manufacturer. The TiV xerogel (before calcination) already exhibits the diffraction pattern of crystalline anatase. However, the peaks are broad and less resolved. It is the calcination step that provokes the formation of a well defined crystalline anatase phase. The estimated size of the anatase domains increases from 5 nm for the xerogel samples to 14–15 nm for the calcined sol–gel samples, independently of the  $V_2O_5$  loading. The size of these anatase crystallites is thus consistent with the size of the elementary particles evidenced in Fig. 2c and d.

Chlorine ( $\sim 2.5$  at%) is detected by XPS at the surface of the xerogels (Table 3). Calcination results in the removal of most of it since the Cl signal is reduced to about 10–15% of the initial value found on the xerogels. The residual contamination ( $\sim 0.3$  at%) is

although well above the detection limit of XPS (0.01 at%). This residual Cl surface contamination has to be related to the nature of the precursors used in the preparation method.

The xerogel is characterized by a very high C surface content (27 at%), exceeding markedly the values corresponding to usual C contamination typically found on Ti/V based systems (usually between 15 and 20 at% [14,41,42]). The high carbon concentration in the xerogel sample has to be correlated with the presence of residual O'Pr groups. Calcination results in the removal of these organic groups as attested by the drop in the carbon atomic surface concentration. The remaining C can then be attributed to usual organic contamination always present at the surface of catalysts that have been contacted with ambient conditions.

The atomic surface concentrations of V and Ti increased as a result of calcination (Table 3). This could be attributed to the cleaning of the inorganic surface through the removal of organic and chlorinated precursor residues. However, Ti surface content only increased slightly while V surface content was multiplied by a factor 3 in the in SG-TiV3 sample. As a result of calcination, the surface is obviously enriched in V. In order to better describe this effect, the V/Ti ratio is given in Table 3. The obvious increase of this ratio evidences the fact that V oxide species migrate toward the surface of Ti oxide as a result of the treatment at  $500^\circ\text{C}$ . This has to be correlated to the fact that the temperature at which the calcination has been performed ( $500^\circ\text{C}$ ) is well above the Tammann temperature of  $V_2O_5$  ( $209^\circ\text{C}$ ). The Tammann temperature – defined as the melting temperature (in K) divided by two – is an empirical parameter corresponding roughly to the temperature at which solid defects are abundant enough to allow bulk mobility. Above this temperature, solids are potentially subjected to phenomena where displacements of atoms in the solid are required (sintering, migration, diffusion, etc.). The limited solubility of V oxide in anatase is the driving force for the segregation of V towards the surface of the material. Note also that, as expected, the V surface concentration and the V/Ti ratio increase with the  $V_2O_5$  nominal loading.

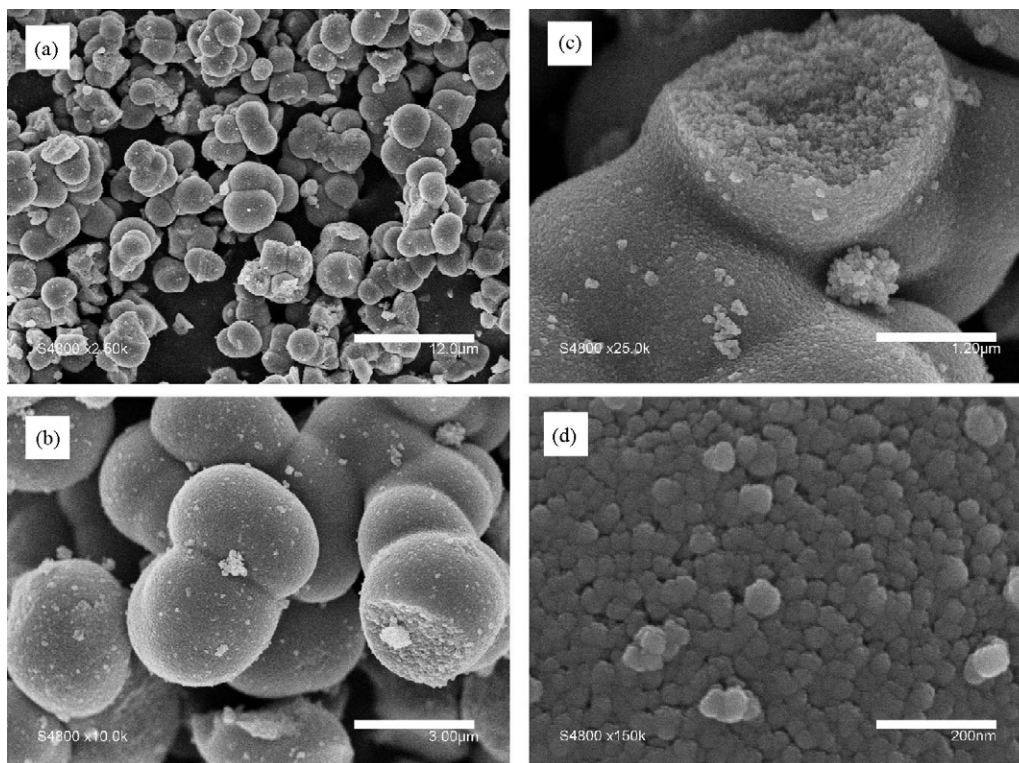


**Fig. 2.** SEM micrographs of SG-TiV3 at different magnitude. The white scale bars represent 12  $\mu\text{m}$ , 3  $\mu\text{m}$ , 1.2  $\mu\text{m}$  and 200 nm, respectively for micrographs (a), (b), (c) and (d).

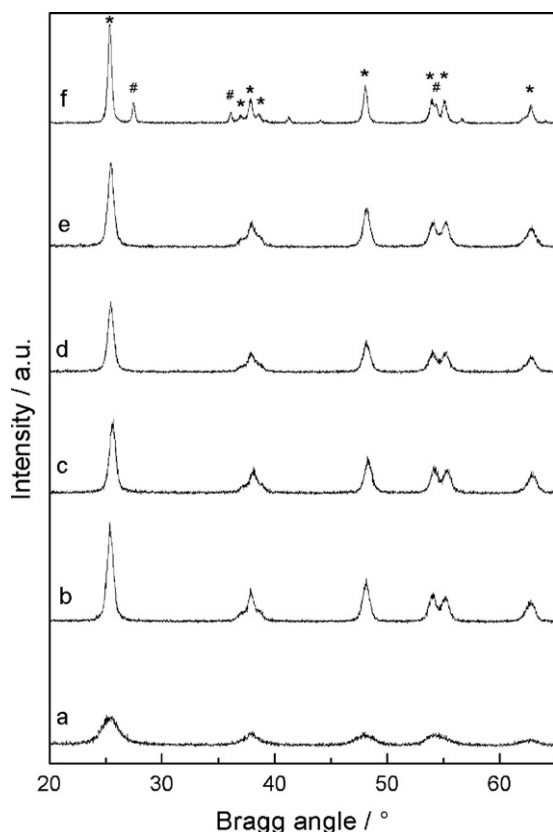


**Fig. 3.** XRD diffractograms of (a) SG-TiV3 xerogel (before calcination); (b) SG-TiV3; (c) SG-TiV3 after catalytic test; (d) SG-TiV5; (e) SG-TiV10 and (f) WI-TiV. Anatase and rutile diffraction lines are marked with "\*" and "#", respectively.

The surface composition of SG and WI catalysts might be compared, bearing in mind the actual composition of each catalyst, as presented in Table 2. The V/Ti ratio for the SG-TiV5 (0.13) is lower than the value found for the WI-TiV5 catalyst (0.17) while both catalysts have approximately the same overall composition. This is not surprising since in WI samples vanadium is deposited onto the TiO<sub>2</sub> surface and all V atoms are supposed to be detected by XPS. On the other hand, in SG samples, V is brought to the surface of the catalyst starting from the bulk of the homogeneous mixed xerogels. It can be inferred that even if the segregation of V at the surface of the SG sample obviously takes place, the phenomenon is actually not complete and part of the V atoms remained in the bulk of the material.

The V 2p<sub>3/2</sub> XPS peak of TiV3 before calcination (xerogels), calcined and spent (after catalytic test) are shown in Fig. 4. The increase in the intensity of this peak after calcination is obvious. Calcination also modified the binding energy (BE) of the V 2p<sub>3/2</sub> peak. It could be stated that the shift depicts vanadium atoms at different oxidation level. However, when involved in the preparation vanadium atoms are already at the V<sup>5+</sup> oxidation level and there is apparently no reason to believe that reduction would occur

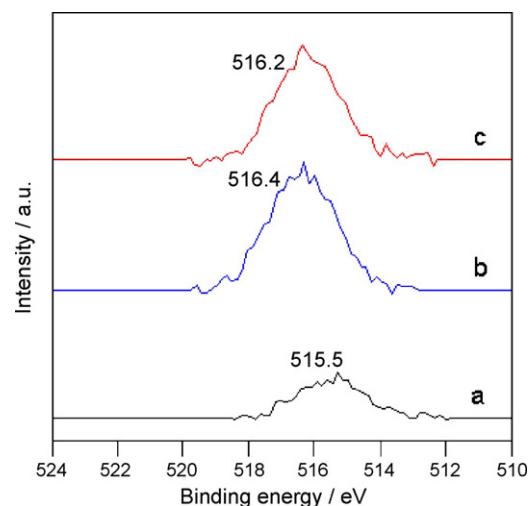


**Fig. 4.** V 2p<sub>3/2</sub> peaks of (a) SG-TiV3 xerogel (before calcination) (b) calcined SG-TiV3 and (c) spent SG-TiV3 (after catalytic test). The peaks have been normalized so that their surface is proportional to the atomic V surface concentration measured on each sample.

during the synthesis or storage of the material. This shift is linked to the environment in which the V<sup>5+</sup> species are located. The position of V<sup>5+</sup> is usually given in the literature for V<sub>2</sub>O<sub>5</sub> oxide: 517.0 to 517.2 eV [44–46]. Also on the WI samples used here and extensively described in the literature [1,4,5,14,20,42,47] the BE of the V 2p<sub>3/2</sub> peak is always found between 517.0 eV and 517.1 eV (see Fig. 5). In that case, a layer of V oxide is formed in which mainly V–O–V bonds are formed. On the other hand, in SG xerogels (before calcination), the occurrence of V–O–Ti bonds is favoured, due to the intrinsic mechanism of non-hydrolytic sol–gel chemistry – in which all alkoxide precursors react with approximately the same kinetics. The electronegativity of V and Ti are respectively 1.63 and 1.54, meaning that Ti attract electrons less than V does. So when a V<sup>5+</sup> is linked (through an O atom) to a Ti<sup>4+</sup> cation instead of being linked to another V<sup>5+</sup>, its electron density is

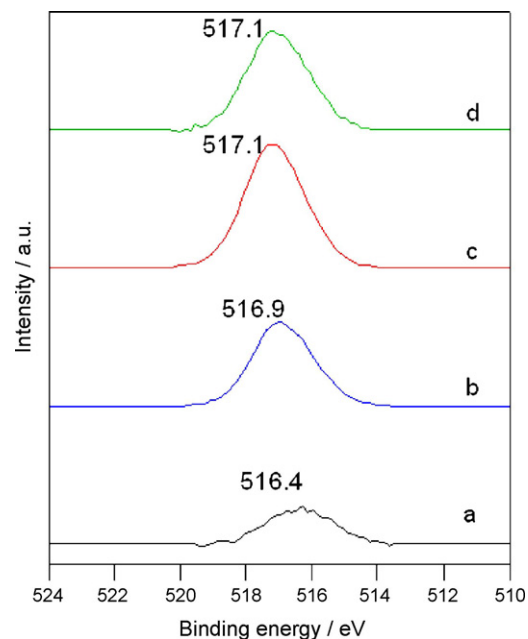


**Fig. 5.** V 2p<sub>3/2</sub> peaks of (a) SG-TiV3 (b) SG-TiV5, (c) SG-TiV10 and (d) WI-TiV5 catalysts. The peaks have been normalized so that their surface is proportional to the atomic V surface concentration measured on each sample.

**Table 3**  
XPS atomic surface concentrations and ratios.

		V (at%)	C (at%)	Cl (at%)	Ti (at%)	V/Ti
SG-TiV3	Fresh	0.4	27.4	2.7	17.1	0.02
	Calcined	1.2	16.8	0.3	21.0	0.06
	Used	1.1	20.7	0.6	20.5	0.05
SG-TiV5	Calcined	2.8	13.8	0.2	21.6	0.13
SG-TiV10	Calcined	4.1	16.6	0.2	19.2	0.22
WI-TiV5	Calcined	3.3	19.5	0.0	19.2	0.17

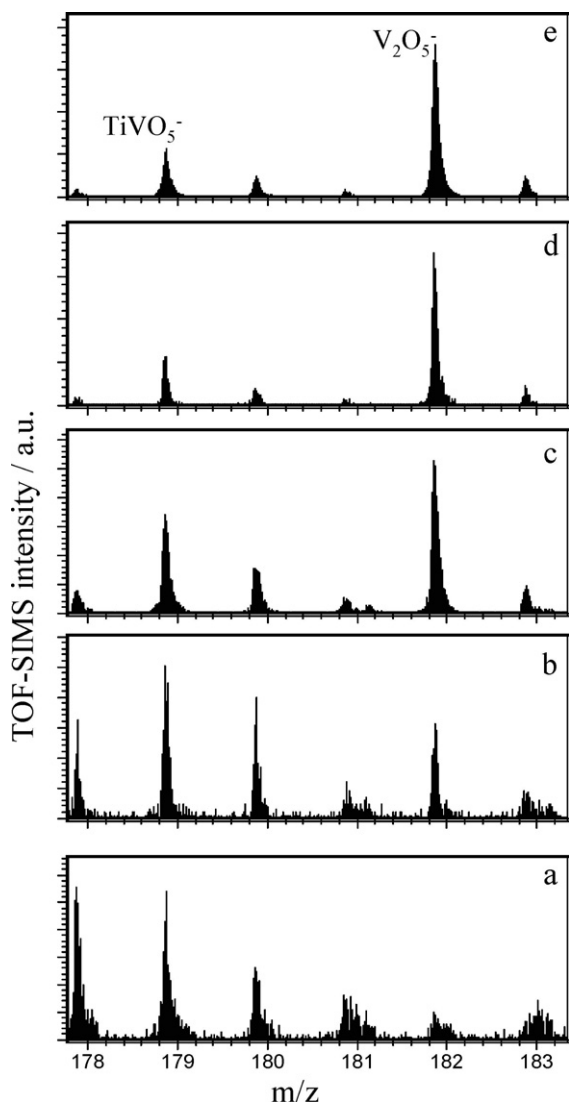


**Fig. 6.** Part of the negative TOF-SIMS spectra obtained on (a) SG-TiV3 xerogel (before calcination), (b) SG-TiV3, (c) SG-TiV5, (d) SG-TiV10 and (e) WI-TiV5. Each spectrum was recorded at least four times and the relative intensity of the peaks did not vary significantly.

higher. As a result the BE of the V  $2p_{3/2}$  XPS peak decreases. Note that in catalysts prepared by grafting of vanadia on titania, in which V–O–Ti bonds are also predominant (especially at low V loading), the reported BE values for the V  $2p_{3/2}$  XPS are also relatively low (e.g. 516.3 eV [48]). After calcination of the xerogel, the V  $2p_{3/2}$  peak shifts to higher BE values, suggesting again that calcination led to the migration of V species toward the surface along with an increase in the proportion of V–O–V bridges. In SG-TiV samples with higher loading, the position of the V  $2p_{3/2}$  XPS peak is further shifted towards higher BE values, closer to the usual position for  $V^{5+}$  in a  $V_2O_5$  environment (Fig. 5). This is in agreement with the presence of higher amount of V–O–V bridges when the V surface concentration increases.

These observations can be correlated with the properties of the outermost surface as probed by TOF-SIMS measurements. More precisely, the relative amount of two cluster ions detected in the negative TOF-SIMS spectra has been followed (Fig. 6). The presence of the  $V_2O_5^-$  ion ( $m/z = 182$ ) has to be correlated with surface species where V–O–V bridges occur (V oxide in the form of vanadium oxide crystallites or oligomers). The presence of the  $TiVO_5^-$  ions ( $m/z = 179$ ) reveals the occurrence of V–O–Ti

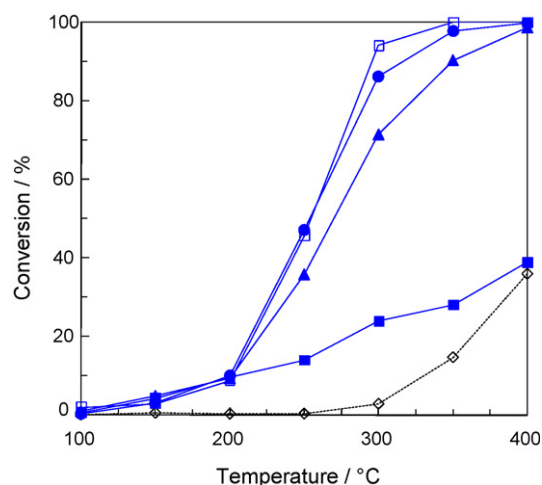


**Fig. 7.** Benzene light-off curves obtained with (◇)  $TiO_2$  (P25 Degussa support), (■) SG-TiV3, (▲) SG-TiV5, (●) SG-TiV10 and with (□) WI-TiV.

bridges. In WI-TiV5, a high proportion of  $V_2O_5^-$  is detected, consistent with the fact that a  $V_2O_5$  phase is formed at the surface of  $TiO_2$ . Nevertheless,  $TiVO_5^-$  ions are also detected, showing that chemical bonds have been formed during the WI preparation. On the other hand, in the xerogel (before calcination) there is a high proportion of  $TiVO_5^-$  ions and the contribution of  $V_2O_5^-$  is very low, which is consistent with vanadium atoms dispersed into the titania matrix. The calcination leads to an increase in the V surface concentration (as already described from XPS) and in an increase in the proportion of  $V_2O_5^-$  ions in the SG-TiV3 catalyst. In the SG samples with higher loading, the proportion  $V_2O_5^-$  ions further increases, consistent with the formation of more V–O–V bonds at the surface of the catalyst. The spectrum of SG-TiV10 appears quite similar to the spectrum of WI-TiV5.

### 3.2. Activity measurements

The performances of the SG-TiV3 in the total oxidation of benzene are quite poor (Fig. 7). Even at 400 °C, the conversion only reaches 40%. When the  $V_2O_5$  loading is increased to 5% and 10%, a significant increase in the catalytic performances is observed. The temperature at which the conversion reaches 50% ( $T_{50}$ ) is 270 °C for SG-TiV5 catalyst and 254 °C for SG-TiV10 catalyst. On the basis of the  $T_{50}$ , this catalyst is as efficient as the reference catalyst prepared by WI. It compares very well with previous reports of the literature for the total oxidation of benzene using  $V_2O_5/TiO_2$  catalysts prepared by classical methods [1].

### 3.3. Spent catalyst characterization

The catalytic test did not provoke any change in the crystallographic state of the catalysts. No formation of V crystalline phase and no collapse of the anatase structure is observed. This is showed for SG-TiV3 in Fig. 3 and was also checked for all the formulations investigated in this study. The V/Ti XPS ratio (Table 2) and the position of the V  $2p_{3/2}$  XPS peak (Fig. 4) are not affected either by the catalytic test. Calcined catalysts have a very low chlorine surface content, arising from the preparation method itself (incomplete removal of chloride moieties). During the test, this remaining contamination is not removed as the Cl surface concentration remains roughly unchanged (Table 2). A small increase in the C surface content is observed on the spent catalysts. This is also classically observed on WI samples [1].

## 4. Discussion

### 4.1. Requirements for application as VOC total oxidation catalyst

The non-hydrolytic route used in this study to prepare TiV catalysts offers a very good control of composition, as attested by the excellent agreement between expected and experimental compositions (Table 2). This is an important condition that makes non-hydrolytic sol–gel chemistry a reliable route for the production of mixed oxides with the desired composition.

The texture of the catalysts is also of primary importance. For being used as VOC total oxidation catalysts, the solids should preferably be mesoporous. Excessive microporosity is deleterious because the pollutants would not have the opportunity to reach the smallest pores. This is particularly true for bulky compounds – like dioxins – and for the typically very high space velocities encountered in VOC abatement applications. The catalysts prepared by non-hydrolytic sol–gel obviously meet these requirements (Table 1 and Fig. 1). The relatively narrow pore size distribution of SG catalysts is explained by the fact that the micronic spherical beads in Fig. 2 are formed by the packing of well-calibrated non-porous nanoparticles about 10–25 nm in size.

The crystallographic structure of the titania-based catalysts presented in this study is based on anatase (Fig. 3). This phase is recognized as the best suited for titania-supported  $V_2O_5$  total oxidation catalysts because the wetting of  $V_2O_5$  on  $TiO_2$  is optimal [49]. So the fact that non-hydrolytic condensation reactions leads to the exclusive formation of anatase even after calcination at 500 °C is important.

### 4.2. Distribution and environment of vanadium species

As shown by chemical analysis, the expected amount of vanadium is present in the SG samples but no crystalline vanadium oxide is detected in XRD experiments. XPS and TOF-SIMS experiments give valuable information on the location of these amorphous vanadium oxide species.

The “surface V/Ti ratio” found in XPS for the SG-TiV3 xerogel is 0.023 (Table 3), which fits closely the expected “bulk V/Ti ratios” calculated from the amount of reactant involved in the preparation ( $=0.024$ ). In addition, almost no  $V_2O_5^-$  ions are detected in TOF-SIMS experiments and the BE of the V  $2p_{3/2}$  XPS peak is low. Accordingly, the xerogels obtained by non-hydrolytic sol–gel appear homogeneous, with V atoms statistically dispersed in a titania matrix and linked to Ti atoms through Ti–O–V bonds, as shown by the abundant  $TiVO_5^-$  ions in the TOF-SIMS spectrum.

The calcination treatment completely modifies the dispersion of V in the catalysts. Both the V surface concentration and the V/Ti ratio increase (Table 3), which shows that V species have migrated toward the surface of the catalyst. This phenomenon has already been evidenced in V–Ti systems [50] and can be explained by the limited solubility of V oxides in  $TiO_2$  and the low Tammann temperature of  $V_2O_5$ . As a result of calcination, the homogeneous xerogels are converted into “heterogeneous” oxides with a high proportion of the V atoms close to the surface. The migration toward the surface of V atoms seems to be quite effective, but part of the vanadium is probably lost in the bulk of the material, as inferred from the comparison with the surface composition of WI-TiV5. Conversely, nearly complete migration of Mo atoms toward the surface was observed in a mixed Mo–Si–Al oxide obtained by non-hydrolytic sol–gel [40].

The calcination also leads to modifications in the environment of V atoms. Both the increase in the relative proportion of  $V_2O_5^-$  ions (Fig. 6) and the shift of the V  $2p_{3/2}$  XPS peak to higher BE (Fig. 4) are consistent with the formation of oligomeric vanadate species at the expense of isolated V species.

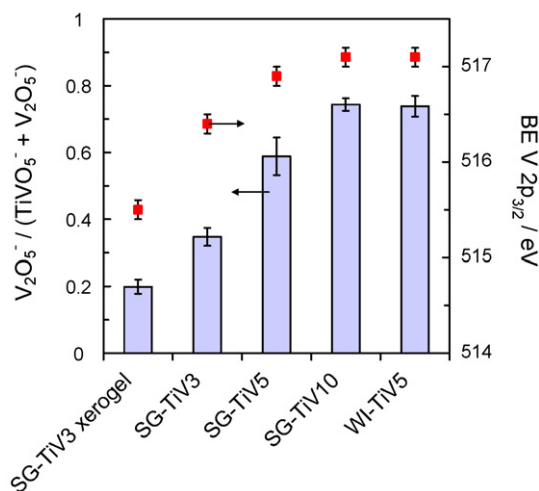


Fig. 8. Correlation between the proportion of oligomeric vanadate species estimated from TOF-SIMS data (columns) and the XPS V  $2p_{3/2}$  binding energy (■).

In the same way, TOF-SIMS and XPS data indicate that the proportion of oligomeric vanadate species in the SG catalysts increases with the  $V_2O_5$  loading. Fig. 8 was drawn in order to visualize the link between the V  $2p_{3/2}$  BE and the ratio  $V_2O_5^- / (TiVO_5^- + V_2O_5^-)$ . An evident correlation is found: when the proportion of V–O–V bonds increases at the expense of V–O–Ti bonds, the BE of the V  $2p_{3/2}$  XPS peak increases. In the case of SG-TiV3, after calcination the surface concentration of V remains low and the vanadium species are mostly isolated, monomeric species. When the  $V_2O_5$  loading increases, the migration of V atoms leads to increasing vanadium surface concentration and the formation of oligomeric V species is favoured. While SG-TiV10 and WI-TiV5 differ in terms of  $V_2O_5$  weight loading and V surface concentration, the environment of V atoms appear quite similar from XPS and TOF-SIMS experiments.

### 4.3. Catalytic performances

Even if the migration of V toward the surface occurs as a result of appropriate calcination conditions, part of the active phase remains in the bulk of the particles, thus not accessible to the reactants. Accordingly, higher  $V_2O_5$  loadings are necessary in the case of sol–gel catalysts to obtain a similar V surface concentration and catalytic performances. Comparing the performances of SG and WI catalysts on the basis of their V surface concentration (or V/Ti ratio) is thus more relevant than comparing on the overall loading.

As shown in Fig. 9, the temperature at which the conversion reaches 40% decreases sharply when the V/Ti ratio increases from 0.06 (SG-TiV3) to 0.13 (SG-TiV5). Then, only a limited increase in activity is seen when this value is further increased (up to 0.22 for SG-TiV10). Interestingly, the similarity of SG-TiV10 and WI-TiV5 in terms of surface chemical environment (Fig. 8) translates into similar catalytic performances (Fig. 7).

The catalytic performances clearly do not vary linearly with the V surface concentration. The low activity of SG-TiV3 in comparison with SG-TiV5, SG-TiV10 and WI-TiV5 should actually be correlated to the different nature of the V surface species in these samples. The well-spread, mostly isolated V surface species anchored to the Ti oxide matrix found in SG-TiV3 appear much less active than the oligomeric vanadates species found in SG-TiV5, SG-TiV10 and WI-TiV5.

Finally, it must be noted that the crystallographic structure of SG samples, V surface concentration and V environment are not affected by the catalytic tests performed up to 400 °C (Table 3, Fig. 4). Prolonged catalytic tests are required to investigate the

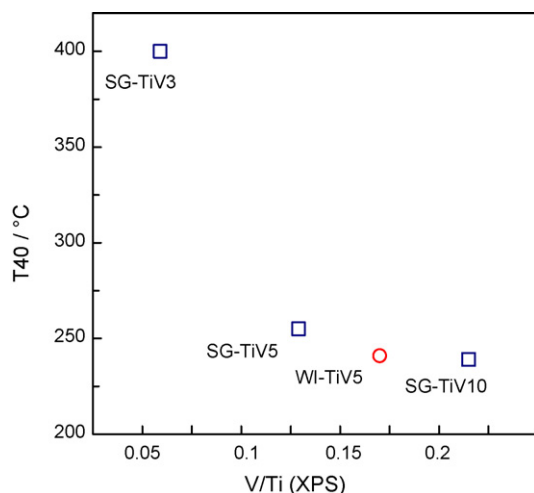


**Fig. 9.** Variation of the T40 (temperature at which the conversion reaches 40%) as a function of the V/Ti ratio determined by XPS for (□) the SG and (○) the WI catalysts.

long-term stability of our catalysts; however, no deactivation was observed during the tests performed here.

The Cl contamination found at the surface of SG samples is not removed during catalytic tests; this Cl contamination is not a problem for  $V_2O_5$ -based catalysts as they were reported to remain very active in the presence of Cl [14]. Although a similar resistance against chlorine poisoning can be expected for the catalysts presented here, further testing would be needed before proposing them for chlorinated pollutants (e.g. dioxins) abatement.

## 5. Conclusions

This work investigated the possibility to prepare efficient VOC total oxidation catalysts through a non-hydrolytic sol-gel route. Our results show that non-hydrolytic sol-gel is an appropriate method for the one-step synthesis of efficient catalysts based on  $V_2O_5$  and  $TiO_2$  with controlled composition and texture, starting from low cost chloride precursors. The mesoporous solids obtained are built of nanoparticles aggregated in spherical grains a few micrometers in size. Calcination of the homogeneous mixed xerogels leads to the migration of most vanadia species toward the surface of the anatase nanoparticles, resulting in a high surface concentration of active phase. This migration was monitored using XPS measurements.

Benzene total oxidation was used as a model reaction and showed that the activity of these catalysts depended on the concentration and on the nature of surface vanadium species. XPS and TOF-SIMS experiments suggested that oligomeric vanadates formed at high  $V_2O_5$  loadings are more efficient than isolated  $VO_x$  species formed at low  $V_2O_5$  loadings.

## Acknowledgments

This work was initiated and supported by the “FAME” Network of Excellence of the EU 6th FP. The authors gratefully acknowledge the Université catholique de Louvain, the Fonds National de Recherche Scientifique (FNRS) in Belgium, the Ministère de l’Enseignement Supérieur et de la Recherche and the Centre National de la Recherche Scientifique (CNRS) in France for financial support. D.P. Debecker acknowledges the FNRS for its Research Fellow position. R. Delaigle thanks the FRIA for its PhD Student position. The involvements of the Unité de catalyse et chimie des matériaux divisés in the “Inanomat” IUAP network sustained by the “Service public fédéral de programmation politique scientifi-

que” (Belgium) and in the Cost Action D41 sustained by the European Science Foundation are also acknowledged.

## References

- [1] R. Delaigle, D.P. Debecker, F. Bertinchamps, E.M. Gaigneaux, *Top. Catal.* 52 (2009) 501–516.
- [2] S. Albonetti, G. Baldi, A. Barzanti, A.L. Costa, J.E. Mengou, F. Trifiro, A. Vaccari, *Appl. Catal., A* 325 (2007) 309–315.
- [3] L. Lazar, H. Koser, I. Balasanian, F. Bandrabur, *Environ. Eng. Manage. J.* 6 (2007) 13–20.
- [4] F. Bertinchamps, A. Attianese, M.M. Mestdagh, E.M. Gaigneaux, *Catal. Today* 112 (2006) 165–168.
- [5] F. Bertinchamps, M. Treinen, P. Eloy, A.M. Dos Santos, M.M. Mestdagh, E.M. Gaigneaux, *Appl. Catal., B* 70 (2007) 360–369.
- [6] V. de Jong, M.K. Cieplik, W.A. Reints, F. Fernandez-Reino, R. Louw, *J. Catal.* 211 (2002) 355–365.
- [7] E. Finocchio, G. Busca, M. Notaro, *Appl. Catal., B* 62 (2006) 12–20.
- [8] C.E. Hetrick, J. Lichtenberger, M.D. Amiridis, *Appl. Catal., B* 77 (2008) 255–263.
- [9] M. Nacken, S. Heidenreich, M. Hackel, G. Schaub, *Appl. Catal., B* 70 (2007) 370–376.
- [10] K. Everaert, M. Mathieu, J. Baeyens, E. Vansant, *J. Chem. Technol. Biotechnol.* 78 (2003) 167–172.
- [11] K. Everaert, J. Baeyens, *J. Hazard. Mater.* 109 (2004) 113–139.
- [12] J.E. Lee, J. Jurng, *Catal. Lett.* 120 (2008) 294–298.
- [13] K. Everaert, J. Baeyens, *Chemosphere* 46 (2002) 439–448.
- [14] F. Bertinchamps, C. Poleunis, C. Gregoire, P. Eloy, P. Bertrand, E.M. Gaigneaux, *Surf. Interface Anal.* 40 (2008) 231–236.
- [15] C.C. Yang, S.H. Chang, B.Z. Hong, K.H. Chi, M.B. Chang, *Chemosphere* 73 (2008) 890–895.
- [16] F. Bertinchamps, C. Gregoire, E.M. Gaigneaux, *Appl. Catal., B* 66 (2006) 10–22.
- [17] E. Finocchio, M. Baldi, G. Busca, C. Pistarino, G. Romezzano, F. Bregani, G.P. Toledo, *Catal. Today* 59 (2000) 261–268.
- [18] M.A. Larrubia, G. Busca, *Appl. Catal., B* 39 (2002) 343–352.
- [19] F. Bertinchamps, C. Gregoire, E.M. Gaigneaux, *Appl. Catal., B* 66 (2006) 1–9.
- [20] D.P. Debecker, C. Faure, M.E. Meyre, A. Derre, E.M. Gaigneaux, *Small* 4 (2008) 1806–1812.
- [21] F. Chiker, J.P. Nogier, J.L. Bonardet, *Catal. Today* 78 (2003) 139–147.
- [22] B. Schimmoeller, H. Schulz, A. Ritter, A. Reitzmann, B. Kraushaar-Czametzk, A. Baiker, S.E. Pratsinis, *J. Catal.* 256 (2008) 74–83.
- [23] W.J. Stark, K. Wegner, S.E. Pratsinis, A. Baiker, *J. Catal.* 197 (2001) 182.
- [24] X. Zhang, X.G. Li, J.S. Wu, R.C. Yang, Z.H. Zhang, *Catal. Lett.* 130 (2009) 235–238.
- [25] J.P. Balikdjan, A. Davidson, S. Launay, H. Eckert, M. Che, *J. Phys. Chem. B* 104 (2000) 8931–8939.
- [26] S. Djerad, L. Tifouti, M. Crocoll, W. Weisweiler, *J. Mol. Catal. A: Chem.* 208 (2004) 257–265.
- [27] I.M. Pearson, H. Ryu, W.C. Wong, K. Nobe, *Ind. Eng. Chem. Prod. Res. Dev.* 22 (1983) 381–382.
- [28] C.B. Rodella, R.W.A. Franco, C.J. Magon, J.P. Donoso, L.A.O. Nunes, M.J. Saeki, M.A. Aegerter, A.O. Florentino, *J. Sol-Gel Sci. Technol.* 25 (2002) 75–82.
- [29] C.B. Rodella, R.W.A. Franco, C.J. Magon, J.P. Donoso, L.A.O. Nunes, M.J. Saeki, M.A. Aegerter, V. Sargentelli, A.O. Florentino, *J. Sol-Gel Sci. Technol.* 25 (2002) 83–88.
- [30] C. Hoang-Van, O. Zegaoui, P. Pichat, *J. Non-Cryst. Solids* 225 (1998) 157–162.
- [31] O. Zegaoui, C. Hoang-Van, M. Karroua, *Appl. Catal., B* 9 (1996) 211–227.
- [32] M. Schneider, M. Maciejewski, S. Tschudin, A. Wokaun, A. Baiker, *J. Catal.* 149 (1994) 326–343.
- [33] B.E. Handy, M. Maciejewski, A. Baiker, *J. Catal.* 134 (1992) 75–86.
- [34] M. Schneider, U. Scharf, A. Wokaun, A. Baiker, *J. Catal.* 150 (1994) 284–300.
- [35] P. Kornelak, D.S. Su, C. Thomas, J. Camra, A. Weselucha-Birczynska, M. Toba, M. Najbar, *Catal. Today* 137 (2008) 273–277.
- [36] P.H. Mutin, A.F. Popa, A. Vioux, G. Delahay, B. Coq, *Appl. Catal., B* 69 (2006) 50–58.
- [37] P.H. Mutin, A. Vioux, *Chem. Mater.* 21 (2009) 582–596.
- [38] A.M. Cojocariu, P.H. Mutin, E. Dumitriu, F. Fajula, A. Vioux, V. Hulea, *Chem. Commun.* (2008) 5357–5359.
- [39] O. Lorret, V. Lafond, P.H. Mutin, A. Vioux, *Chem. Mater.* 18 (2006) 4707–4709.
- [40] D.P. Debecker, K. Bouchmella, C. Poleunis, P. Eloy, P. Bertrand, E.M. Gaigneaux, P.H. Mutin, *Chem. Mater.* 21 (2009) 2817–2824.
- [41] D.P. Debecker, F. Bertinchamps, N. Blangenois, P. Eloy, E.M. Gaigneaux, *Appl. Catal., B* 74 (2007) 223–232.
- [42] D.P. Debecker, R. Delaigle, P. Eloy, E.M. Gaigneaux, *J. Mol. Catal. A: Chem.* 289 (2008) 38–43.
- [43] P. Bertrand, L.T. Weng, *Mikrochim. Acta* 13 (1996) 167–182.
- [44] G. Silversmit, D. Depla, H. Poelman, G.B. Marin, R. De Gryse, *J. Electron. Spectrosc. Relat. Phenom.* 135 (2004) 167–175.
- [45] J. Mendialdua, R. Casanova, Y. Barbaux, *J. Electron. Spectrosc. Relat. Phenom.* 71 (1995) 249–261.
- [46] I. Georgiadou, C. Papadopoulos, H.K. Matralis, G.A. Voyiatzis, A. Lycourghiotis, C. Kordulis, *J. Phys. Chem. B* 102 (1998) 8459–8468.
- [47] F. Bertinchamps, M. Treinen, N. Blangenois, E. Mariage, E.M. Gaigneaux, *J. Catal.* 230 (2005) 493–498.
- [48] M.A. Reiche, T. Burgi, A. Baiker, A. Scholz, B. Schnyder, A. Wokaun, *Appl. Catal., A* 198 (2000) 155–169.
- [49] M. Gasior, J. Haber, T. Machej, *Appl. Catal.* 33 (1987) 1–14.
- [50] U. Scharf, M. Schneider, A. Baiker, A. Wokaun, *J. Catal.* 149 (1994) 344–355.